High-Performance and Tailorable Pressure Sensor Based on Ultrathin Conductive Polymer Film

*Qi Shao, Zhiqiang Niu, Michael Hirtz, Lin Jiang, Yuanjun Liu, Zhaohui Wang, and Xiaodong Chen**

Pressure sensors have been used as tactile sensing elements on prosthetic hands and in humanoid robots,[1] employed during minimal access surgery[2,3] and incorporated into smartphones and touch screen devices. More recently, the utilization of touch technology, such as pressure-sensitive artificial skin,[4,5] can even compete with performance of human beings, which are capable of sensing a mass-loading as low as 0.1 g mm^{-2} (or about 1 kPa).[6–9] Despite the exciting development, researchers are still pushing forward and attempting to acquire the capability of detecting pressures lower than 1 kPa for applications with extreme requirements, such as detection of micro-sized objects.[10] However, such tasks are still challenging.[6,11]

Categorized by principle, resistive,[12–16] capacitive,[17–23] piezoelectric,[24–29] piezoresistive,[30–36] and optical[37–39] pressure sensors, have been developed over the past decades. Capacitive pressure sensors based on microstructured polydimethylsiloxane (PDMS) films demonstrate sensitivity up to 8.3 kPa^{-1},[23] but impurities and other contaminants may cause a change of the dielectric constant and affect the sensors' performance.[21,40] Piezoelectric pressure sensors offer higher sensitivity but are unable to measure static load.[41–43] Based on conductive rubber, resistive pressure sensors show large hysteresis and poor sensitivity in low pressure region.[44] Nevertheless, development of a novel pressure sensor for the various applications mentioned previously would be critical to detect pressure lower than 1 kPa without reducing sensitivity under static load. According to Holm's theory,[45] contact resistance will change as a power law function of the external force, providing an alternative strategy for tactile sensors at low pressure regions. Up to now, the contact resistance based pressure sensors[46–49] have demonstrated good repeatability with fast response time (in seconds timescale). However, neither sensitivity nor accessible pressure region of the present contact resistance based sensors is sufficient to compete with that of human skin.

Mechanical ductility of the sensor materials, such as carbon based materials,[50–52] ZnO,[53] or composite materials,[54–57] is critical for the performance of a pressure sensor. Moreover, it has also been demonstrated that specific structures fabricated in the sensor enhance its performance. By taking both considerations, herein, we report a high performance and tailorable pressure sensor based on an ultrathin conductive polymer film which is prepared by wet chemistry method. The excellent mechanical and electrical properties of conductive polymers,[58–60] such as polypyrrole (PPy), govern the stable and reproducible response of the pressure sensor under loading and unloading. The design principle of our pressure sensor relies on the variable contact resistance between a gold (Au) micropillar array and the conductive polymer film under different static loading. The power law relationship between contact resistance and pressure guarantees a high sensitivity of the pressure sensor, which possesses a tunable sensitivity from 0.03 kPa^{-1} to 17 kPa^{-1} at pressure regions less than 1 kPa. Even more, the sensor can reach a limit of detection as low as 2 Pa with a pillar diameter of 20 μm. Such performance of pressure sensor even surpasses the capability of human skin, so the sensor can potentially be applied for static detection of micro-sized objects.

The pressure sensor is composed of two key components: an Au micropillar array and a deformable PPy film deposited on a PDMS substrate (**Figure 1**a). The sensor circuit is connected with silver paste and copper wire from each end of the PPy film, and *I–V* measurements were obtained under different amount of loading. For a typical device, the width of the Au micropillar array wafer is designed to be 1 mm wider than that of PPy film underneath to avoid misalignment of the two active components of the pressure sensor. Micropillar arrays have previously been used in cellular mechanics studies[61] and in pressure sensors,[22,23,62] where response and relaxation timescales in the order of millisecond were achieved due to the resultant air gaps between the pillar

Q. Shao,[+] Dr. Z. Niu,[+] Dr. M. Hirtz,
Dr. L. Jiang, Y. Liu, Prof. X. Chen
School of Materials Science and Engineering
Nanyang Technological University
50 Nanyang Avenue, Singapore, 639798
E-mail: chenxd@ntu.edu.sg

Dr. M. Hirtz
Institute of Nanotechnology (INT) and Karlsruhe Nano Micro Facility (KNMF)
Karlsruhe Institute of Technology (KIT), Germany

Z. Wang
Beijing National Laboratory for Molecular Sciences
Key Laboratory of Organic Solids, Institute of Chemistry
Chinese Academy of Sciences, Beijing 100190, China

[+]These two authors contributed equally to this work.

DOI: 10.1002/smll.201303601

NANO MICRO small

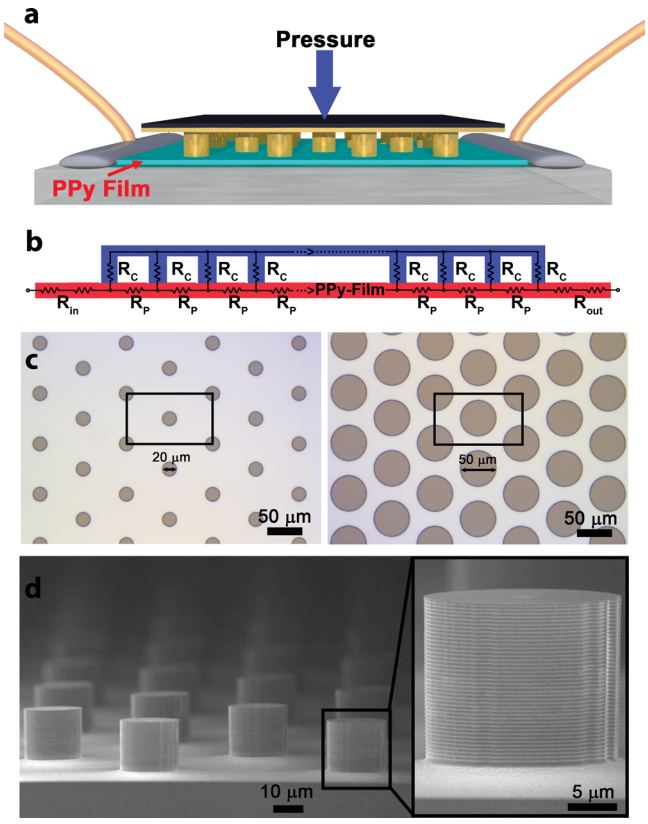

Figure 1. Fabrication of the micropillar array based pressure sensor. a) Schematic drawing of the highly sensitive pressure sensor. The active pressure sensing area is comprised of PPy/PDMS substrate and an Au covered micropillar array. b) The proposed equivalent electrical circuit for a row of columns of such a pressure sensor. c) Optical image of photolithography fabricated patterns. All used pillar patterns have the same unit cell, 70.0 μm × 120.0 μm, but the diameter of the pillars vary from 5 μm to 65 μm. d) A cross section view of a Si micropillar array with the diameter of ~ 20 μm.

and the underneath substrate. The current flow through the device will depend on the contact resistance (R_C) between the Au covered micropillar and PPy film and the resistance of the PPy film (R_P) in between two adjacent pillars (Figure 1b). Therefore, the design for our pressure sensor is based on both, the conductivity of PPy film and the pillar geometry. By varying these two criteria, we can fabricate a pressure sensor with different sensitivities at desirable pressure region.

In a typical pressure sensor, microscale dot patterns were prepared by using conventional photolithography and AZ1518 positive photoresist (Figure 1c). It should be noted that all structures have the same unit cell size, and that only the diameter of the pillars varies, ranging from 5 μm to 65 μm. Pillar patterns with diameter of 20 and 50 μm are shown in Figure 1c as examples, and micrographs of the other pillar patterns are provided in Figure S1, Supporting Information. Deep reactive ion etching of the patterned silicon (Si) wafer followed the completion of photolithography. A cross sectional view of a pillar structure with a pillar diameter of 20 μm is shown in Figure 1d, with the height of each pillar (inset of Figure 1d) measured at 17.0 ± 0.5 μm throughout the whole array. The micropillars are regular and uniform across the full size of the Si wafer, as shown by the highly parallel rows of identically high pillars in scanning electron microscope (SEM) images (Figure 1d). SEM micrographs of the other pillar arrays with different diameters are illustrated in Figure S2. At last, a highly conductive layer of Au (100 nm) on a Cr (10 nm) adhesive layer was deposited by magnetron sputtering, ensuring continuous film coverage on top of the Si micropillar arrays. This operation generates a uniform conduction layer of low resistivity throughout the pillar array, allowing consistent and reproducible device performance. Detailed procedures for chemically depositing PPy films on PDMS substrates are given in the experimental section. The typical thickness of the PPy film in the presented devices is 30 nm as imaged by atomic force microscope (AFM) (Figure S3). Because the Au micropillar arrays are made from Si wafer, which is rigid and flat in nature, there is no need to add additional flat interlinking materials on top of the device for uniform loading. This ensures a complete transfer of applied pressure to the active sensing area without damping, yielding a straightforward pressure-response and makes it easier to describe the underlying mechanism. The PDMS substrate enables elastic deformation of the PPy film, ensuring better contact with the micropillar arrays in response to different pressure loading. Therefore, there are two advantages of having an Au micropillar array and a deformable PPy film as the sensors' key components: one is the direct transfer of pressure loading from the Si-based pillar structure to the PPy film for maximized sensitivity; the other is the fast response and relaxation time due to the air gap introduced by the micropillar arrays.

As an example, the performance of the pressure sensor with a pillar diameter of 20 μm is presented first: *I–V* curves of such a micropillar array based pressure sensor are measured under different loads (**Figure 2**a). This is further elaborated in the plots in Figure 2b. From the data, we can see that the *I–V* characteristics are linear, reflecting the Ohmic behavior of the pressure sensor as a whole. The current increases tremendously with higher pressure loading. Figure 2b shows the relative change of resistance of the device under different pressure loads. The relative resistance change decreases linearly for a pressure range from 0 to 0.35 kPa. Initially, in a state without loading, the pressure sensor shows maximum resistance. When pressure is applied, the contact resistance between the Au covered micropillars and the PPy film decreases, leading to a decline in the total resistance of the device. Such decline is due to more and more current flowing through the low resistance gold film instead of the higher resistance PPy film. Eventually, this tendency saturates with applying higher loads. This saturation process is preferable in real-life applications, as it increases the sensor's accessible pressure range to higher loads, at which high sensitivity is not required. The pressure sensitivity *S*,[22] as shown in the following equation, can be defined as the slope in the linear region of the curve in the inset of Figure 2b:

$$S = \frac{\delta \frac{\Delta R}{R_0}}{\delta P} = \left(\frac{1}{R_0}\right) \cdot \delta R / \delta P \quad (1)$$

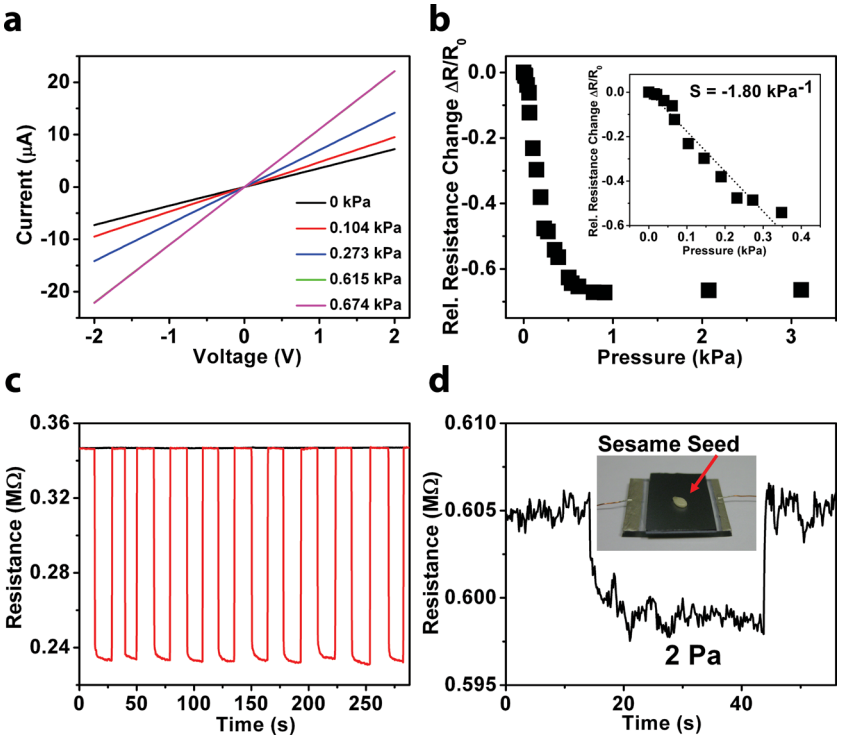

Figure 2. Performance of the pressure sensor with the pillar diameter of 20 μm. a) *I–V* curves of the device under different amount of pressure loading. b) Pressure-response curve for the device. The slope of the relative resistance change below 0.35 kPa range is –1.80 kPa^{-1}. The minus sign means the resistance is decreased with increasing pressure. c) Relaxation and response curve for the device, shown is the resistance change on placing and removing a loading of 1 kPa. d) Relaxation and response curve for the device after loading 2 Pa (equivalent to the weight of a sesame seed put on a pressure sensor with an area of 1 × 1.5 cm^2) and unloading.

where P denotes the applied pressure, and R and R_0 denote the resistances with and without applied pressure, respectively. The contact resistance based pressure sensor shows a sensitivity of –1.80 kPa^{-1} (the minus sign indicates decrease of resistance with higher pressure loading). Besides sensitivity, another important requirement for high-performance pressure sensor is a fast response and relaxation time, as shown in Figure 2c (at a load of 1 kPa). Due to the excellent elastic deformation of the PDMS substrate and the air gaps introduced by the pillar structure, the response and relaxation time corresponding to loading and unloading of the sensor is in a timescale of decisecond. Since the weight is put onto the pressure sensor manually, the response and relaxation time is limited by operational parameter. With an automated control of loading and unloading process, the sensor is expected to achieve response and relaxation time less than decisecond timescale. From the aspect of detection limit, the micropillar array based pressure sensor can reliably detect the placement or removal of an ultra-small object such as a sesame seed (weight: 2 mg), which corresponds to a very small pressure of only 2 Pa static loads (considering the total pillar area as the effective area).

As the sensitivity requirements at different pressure regions vary depending on applications, we further investigated how the device design criteria influence the sensitivity of the pressure sensor. Specifically speaking, both the conductivity of the PPy film and the micropillar geometry are critical in influencing the performance of the pressure sensor, which will be illustrated in details in the following. On one hand, the performance of the pressure sensor depends on the conductivity of the PPy film. PPy films with different conductivity were obtained by treatment with sodium hydroxide (NaOH) solution at 0.1 M concentration for different time lengths, leading to reduction of conductivity due to interruption of conjugated bond.[63–66] The conductivity of a PPy film without base treatment is 100 S m^{-1}, and it decreases to 1 S m^{-1} and 10 S m^{-1} after the film is soaking in base solution for appropriate time lengths. The relationship between the conductivity of the PPy film and the sensitivity of the pressure sensor has been shown in Figure S4. The plot reveals that raising the conductivity of the PPy film also increases the pressure sensor's sensitivity. Therefore, PPy films with 100 S m^{-1} conductivity were used in all subsequent experiments.

Furthermore, we investigated the influence of the Au covered micropillar array geometry on the overall resistance as well as on the device performance by increasing the pillar diameter, while keeping the same pillar center-to-center distance. Double logarithmic plots of overall resistance versus pressure for pillar diameters from 5 μm to 65 μm are presented in **Figure 3**a, which reveals a shift of the resistance curves from upper right (high pressure/high resistance regime) to lower left (low pressure/low resistance regime) with increasing pillar diameter. This can be understood because when increasing the diameter of the pillars, the force that is exerted on the contact towards the PPy film for a given pressure applied will be increased, leading to a lower R_C for the same pressure P. Due to the reduced R_C, the overall resistance of the device is lowered already at lower pressures for larger pillar diameters compared to structures with smaller pillar diameters, hence the curves shift to the lower left region for increasing pillar diameter. The error bars in the graph represent one standard deviation out of 7 devices averaged, showing the good reproducibility of the devices. Furthermore, the device performances with different pillar sizes are given in Figure 3c, with a plot of relative resistance change versus pressure. The relative resistance change is increased with increasing pillar size as applied pressure is kept constant. In order to have a better comparison for pillar diameters from 5 μm to 65 μm, despite the small overlap in experimental accessible pressure range for the extreme cases of pillar diameter, only few data points are selected for the 5 μm plot in Figure 3c. The full data set for the 5 μm pillar diameter case is shown in Figure S5. In order to express the relationship between the device performance and pillar size in a more straightforward

NANO MICRO small

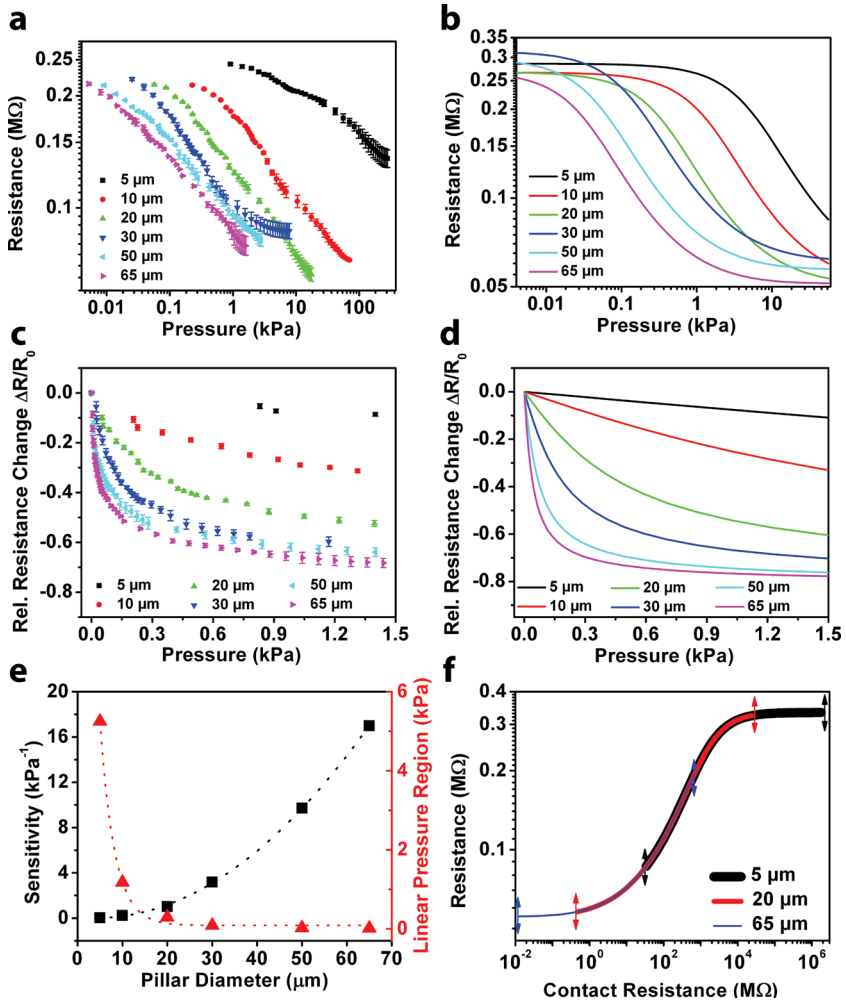

Figure 3. Experimental and simulated impact of change in pillar diameter towards device performance. a) Experimental data and b) model prediction in a double logarithmic plot of total resistance versus pressure, with different pillar sizes from 5 µm to 65 µm. c) The experimental data and d) model prediction for relative resistance change versus pressure, showing increased relative resistance change with increasing pillar size. e) The sensitivity derived from the linear region of the relative resistance versus pressure curves for different pillar diameters, and the value of the pressure range covered by each linear region. The dotted lines are just guiding. f) The relationship between total resistance and contact resistance for different pillar size as derived from numerical simulations. Curves for pillar sizes with 5 µm, 20 µm and 65 µm diameters are shown in this graph.

way, a plot of sensitivity with respect to pillar size is shown in Figure 3e. The graph shows that the sensitivity is significantly increased with increasing pillar size, ranging from 0.03 kPa^{-1} to 17 kPa^{-1}. However, the linear pressure region is also tremendously decreased due to larger pillar size, which is observable from Figure 3c as well. This opens up the opportunity for tailorable design of the sensor devices by choosing the pillar diameter according to the desired sensitivity and pressure ranges.

In order to confirm the contact resistance between the Au covered micropillar and the PPy film as the underlying mechanism for our pressure sensor, a numeric simulation based on the geometry shown in Figure 1a has been proposed. The system can be seen as a parallel circuit of identical rows of pillars running from one electrode to the other. By this partitioning, the single rows can be calculated as a network of resistances R_C and R_P (Figure 1b) and the response of the whole system can be derived by a parallel composition of the single row resistances. Applying Kirchhoff's laws to these networks, a term for the overall resistance of the device can be derived, which is dependent on the balance of R_C and R_P (see Supporting Information for a detailed derivation). While R_P remains constant for a given PPy film and distance of pillars in a device, R_C is highly dependent on the pressure applied to an Au covered pillar-PPy contact: Holm's theory[45] predicts a power law relationship between the applied pressure and the contact resistance as shown in the following equation:

$$R_C(P) = k \cdot \left((P + P_{in}) \cdot A_C\right)^{-n} \quad (2)$$

P is the applied pressure to the pillars, P_{in} is the initial pressure present due to the inherent weight of the pillar structure, and A_C is the area of one pillar in contact with the PPy film. k and n are variables depending on the properties of a particular device. By 4-point probe measurements, we confirmed that the intrinsic resistance of the Au covered pillar array and the contact resistance between the silver paste and the PPy film are small compared to the other resistance components R_P and R_C and can therefore be neglected. The only remaining resistance significantly influencing the total resistance in the device is that of the PPy film parts outside of the contacting Au covered pillar array structure. We define these as R_{in} and R_{out}, respectively, and they are given by the specific resistivity of the PPy film and the length of the PPy film in the device not covered by the pillar structure. In short, the important components that influence the overall device resistance are then only R_C, R_P, R_{in} and R_{out}. The device characteristics can therefore be understood as the outcome of the specific balance between R_P and R_C in the Ohmic networks of the device with a highly pressure sensible R_C, modulated by the resistances R_{in} and R_{out}. Numerical simulations based on this model, taking into account the geometrical dimensions (pillar diameter and distance between pillars) and named resistance components can accurately replicate all observed device characteristics as is shown in the comparisons of theoretical predictions and experimental outcomes in the following discussion of results. A more detailed discussion of the model itself as well as different parameter sweeps can be found in the Supporting Information.

Numeric simulations based on the proposed model can neatly replicate the effects observed in the experiment; this is shown in Figure 3b. Though a total quantitatively match is not achieved with this simple model, the qualitatively outcome is very well predicted. Not only the overall shape, shifting, and general sequence of the curves is replicated, but also additional shifts up and down caused by slight differences in the PPy film resistance of different devices, causing overlaps of the curves (most evident in the case of the curves for 20 μm and 30 μm) are in agreement. It should be noted, that the simulated curves (Figure 3b and 3d) were generated with the same values for n and k and the other parameters (geometry of pillar structure and resistance of the PPy film) were all fixed as given by the experimental setup, so after the initial determination of n and k, no additional fitting to experimental data has taken place. Juxtaposing the curves derived from numerical simulations (Figure 3d) again shows a neat agreement with the experimental data, indicating that the system is described in a valid way by our model. It is noteworthy that the relationship between the overall resistance and contact resistance (which is inaccessible for direct experimental observation in our setup) has been analyzed by numerical simulations as shown in Figure 3f. The double logarithmic plot clearly reveals that very small as well as very large pillar sizes, like 5 μm and 65 μm, lead to regions where the overall resistance does not respond sensitively to changes in R_C (plateau regions). However, a pillar with the diameter of 20 μm minimizes this plateau region for a given set of parameters and typical PPy film resistance, and has a highly sensitive response in overall resistance with respect to R_C changes for the whole pressure range. Therefore, pillar diameter should be chosen carefully to ensure maximum sensitivity when designing device parameters.

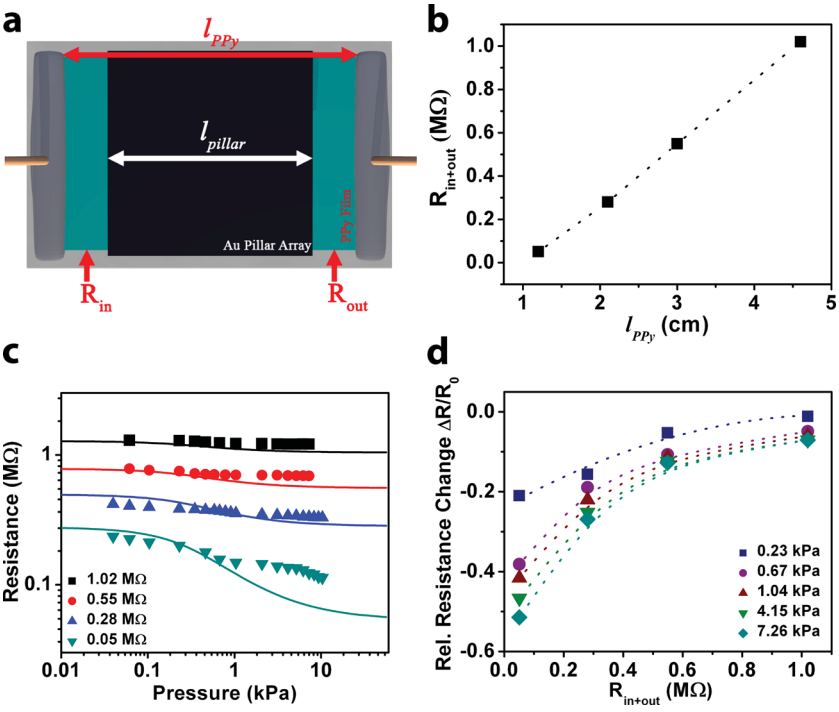

Figure 4. Effect of PPy channel length on sensor performance. a) A top-view of the pressure sensor illustrates the part corresponding to R_{in} and R_{out} on the PPy film. When varying the PPy channel length l_{PPy}, the value of R_{in} and R_{out} changes accordingly. b) By varying the length l_{PPy}, the value of (l_{PPy}- l_{pillar}) also changes, resulting in a linear change of the resistance R_{in+out}. The dotted lines are guiding lines. c) The total resistance versus pressure relationship is shown both with experimental data in dots and curves from numerical simulations under different PPy channel length. d) With decreasing value of R_{in} and R_{out}, the relative resistance change is increased, hence leading to better performance of the device. The dotted lines are guiding lines.

In the proposed electrical circuit, besides the resistance component of R_C and R_P, the resistance of the PPy film extending beyond the Au pillar array, R_{in} and R_{out}, also have a great influence on the overall resistance. Here we define the PPy channel length between the two electrodes as l_{PPy}, and the length of Au pillar array as l_{pillar} indicated in **Figure 4**a. Since we used the Au pillar array with l_{pillar} = 1.0 cm for all the experiments, by changing the PPy channel length l_{PPy}, the PPy film extending outside Au pillar array (l_{PPy} -l_{pillar}) could be varied from 3.6 cm to 0.2 cm. Therefore, the summed up value of R_{in} and R_{out} (R_{in+out}) could be tuned from 1.02 MΩ to 0.05 MΩ by considering the resistivity and specific length of the PPy film. The linear relationship between R_{in+out} and PPy channel length l_{PPy} is shown in Figure 4b; and the influence of PPy channel length or R_{in+out} on the overall resistance is shown in Figure 4c. Both the experimental data and the data derived from the model reveals that with a shorter PPy channel length, or smaller R_{in+out} resistance, the plateau region is decreased, and the linear region is increased correspondingly, which in turn shows a greater response in relative resistance change (Figure 4d). The smaller the R_{in+out} value, the larger the change for the relative resistance, yielding greater sensitivity of the device. Therefore, a smaller R_{in+out} resistance, or in another word, a shorter PPy channel length is preferred when building such a contact resistance based pressure sensor.

In summary, we have described a type of high performance and tailorable pressure sensor that merits the elastic nature of conductive PPy films, as well as air gaps generated from micropillar structures. The high sensitivity at low pressure regions is governed by the variation of contact resistance between the Au covered micropillar array and a deformable PPy film. The sensitivity of the pressure sensor could be tuned from 0.03 kPa^{-1} to 17 kPa^{-1} by varying the pillar diameter accordingly. The behavior of the sensor devices was numerically simulated, giving a more thorough understanding for the underlying principles that generate the sensor response. For the pressure sensor with a pillar diameter of 20 μm, a sensitivity as high as 1.80 kPa^{-1} was achieved in the low pressure region (<0.35 kPa) and the limit of detection was found to be as low as 2 Pa. With this, the performance of the pressure sensor has even surpassed the capability of human skin

NANO MICRO small

in sensing low pressure. Due to their high sensitivity at the low pressure regime, conductive polymer based pressure sensors have the potential to be used for detecting micro-scale objects. Finally, we envisage this contact resistance based sensing mechanism to be applicable for touch screen devices.

Experimental Section

Fabrication of Polypyrrole Film on PDMS: A clean and fluorinated (with Trichloro(1H,1H,2H,2H-perfluorooctyl)silane) 4 inch silicon wafer was placed inside a glass petridish, PDMS (Sylgard 184 pre-mixed with 1/10 crosslinker both from Dow Corning Co.) was poured and annealed at 90 °C for 1 hour. The free standing PDMS film was peeled off from the wafer and cut into the desired size (1.5 cm × 1.5 cm). Before chemically depositing of the PPy film on the surface of the PDMS substrate by oxidizing pyrrole (0.2 M) with iron chloride (0.02 M), PDMS was treated with H_2O/H_2O_2/HCl (in a volume ratio of 5:1:1) for 15 minutes to render it hydrophilic.[67] This was to ensure that the well growth of the N-(3-trimethoxysilylpropyl)pyrrole monolayer on top of it by using a vacuum vapor method to covalently bond with the PPy film in the later process, hence increasing the adhesion between the substrate and the PPy film for robustness.[59] The thickness of the film is well controlled by time, and an optimal duration was found to be 18 minutes leading to continuous and smooth PPy film formation.

Characterization: The structures of the Au covered micropillar array were characterized by field-emission (FE) SEM (JSM-7600F from JEOL). The morphology of the PPy film was characterized by tapping mode AFM (Veeco Multimode SPM system with a NanoScope V control station). The *I–V* characteristics and resistance changes were recorded by a Keithley 4200 Semiconductor Characterization System under different pressure loadings. For the analysis of pressure responses (response and relaxation time), objects with varying weight were loaded and unloaded onto the sensor, and I-t responses were recorded simultaneously.

Supporting Information

Supporting Information is available from the Wiley Online Library or from the author.

Acknowledgements

This work was supported from the National Research Foundation of Singapore (NRF-RF2009–04 and CREATE Programme of Nanomaterials for Energy and Water Management) and Centre of Excellence for Silicon Technologies (Si-COE). M.H. thanks NTU for financial support under the Tan Chin Tuan Fellowship grant.

[1] M. H. Lee, H. R. Nicholls, *Mechatronics* **1999**, *9*, 1.
[2] M. E. H. Eltaib, J. R. Hewit, *Mechatronics* **2003**, *13*, 1163.
[3] C. G. Li, K. Lee, C. Y. Lee, M. Dangol, H. Jung, *Adv. Mater.* **2012**, *24*, 4583.
[4] J. Livage, *Nat. Mater.* **2003**, *2*, 297.
[5] T. Someya, T. Sekitani, S. Iba, Y. Kato, H. Kawaguchi, T. Sakurai, *Proc. Natl. Acad. Sci. USA* **2004**, *101*, 9966.
[6] J. J. Boland, *Nat. Mater.* **2010**, *9*, 790.
[7] D.-H. Kim, N. Lu, R. Ma, Y.-S. Kim, R.-H. Kim, S. Wang, J. Wu, S. M. Won, H. Tao, A. Islam, K. J. Yu, T.-i. Kim, R. Chowdhury, M. Ying, L. Xu, M. Li, H.-J. Chung, H. Keum, M. McCormick, P. Liu, Y.-W. Zhang, F. G. Omenetto, Y. Huang, T. Coleman, J. A. Rogers, *Science* **2011**, *333*, 838.
[8] Z. Ma, *Science* **2011**, *333*, 830.
[9] T. Sekitani, Y. Noguchi, K. Hata, T. Fukushima, T. Aida, T. Someya, *Science* **2008**, *321*, 1468.
[10] K. Subannajui, A. Menzel, F. Güder, Y. Yang, K. Schumann, X. Lu, M. Zacharias, *Adv. Funct. Mater.* **2013**, *23*, 191.
[11] V. Maheshwari, R. Saraf, *Angew. Chem. Int. Ed.* **2008**, *47*, 7808.
[12] M. Hussain, Y. H. Choa, K. Niihara, *J. Mater. Sci. Lett.* **2001**, *20*, 525.
[13] D. Bloor, A. Graham, E. J. Williams, P. J. Laughlin, D. Lussey, *Appl. Phys. Lett.* **2006**, *88*, 102103.
[14] M. Madsen, K. Takei, R. Kapadia, H. Fang, H. Ko, T. Takahashi, A. C. Ford, M. H. Lee, A. Javey, *Adv. Mater.* **2011**, *23*, 3115.
[15] T. Someya, Y. Kato, T. Sekitani, S. Iba, Y. Noguchi, Y. Murase, H. Kawaguchi, T. Sakurai, *Proc. Natl. Acad. Sci. USA* **2005**, *102*, 12321.
[16] T. Sekitani, T. Yokota, U. Zschieschang, H. Klauk, S. Bauer, K. Takeuchi, M. Takamiya, T. Sakurai, T. Someya, *Science* **2009**, *326*, 1516.
[17] W. Hu, X. Niu, R. Zhao, Q. Pei, *Appl. Phys. Lett.* **2013**, *102*, 083303.
[18] Y. Abdi, A. Ebrahimi, S. Mohajerzadeh, M. Fathipour, *Appl. Phys. Lett.* **2009**, *94*, 173507.
[19] T. Takahashi, K. Takei, A. G. Gillies, R. S. Fearing, A. Javey, *Nano Lett.* **2011**, *11*, 5408.
[20] F. Xu, Y. Zhu, *Adv. Mater.* **2012**, *24*, 5117.
[21] J. Kim, T. N. Ng, W. S. Kim, *Appl. Phys. Lett.* **2012**, *101*, 103308.
[22] S. C. B. Mannsfeld, B. C. K. Tee, R. M. Stoltenberg, C. V. H. H. Chen, S. Barman, B. V. O. Muir, A. N. Sokolov, C. Reese, Z. Bao, *Nat. Mater.* **2010**, *9*, 859.
[23] G. Schwartz, B. C. K. Tee, J. Mei, A. L. Appleton, D. H. Kim, H. Wang, Z. Bao, *Nat. Commun.* **2013**, *4*, 1859.
[24] J. Zhou, P. Fei, Y. Gao, Y. Gu, J. Liu, G. Bao, Z. L. Wang, *Nano Lett.* **2008**, *8*, 2725.
[25] S. C. Hung, B. H. Chou, C. Y. Chang, C. F. Lo, K. H. Chen, Y. L. Wang, S. J. Pearton, A. Dabiran, P. P. Chow, G. C. Chi, F. Ren, *Appl. Phys. Lett.* **2009**, *94*, 043903.
[26] Y. Hu, J. Zhou, P.-H. Yeh, Z. Li, T.-Y. Wei, Z. L. Wang, *Adv. Mater.* **2010**, *22*, 3327.
[27] C. Li, P.-M. Wu, L. A. Shutter, R. K. Narayan, *Appl. Phys. Lett.* **2010**, *96*, 053502.
[28] I. Graz, M. Kaltenbrunner, C. Keplinger, R. Schwodiauer, S. Bauer, S. P. Lacour, S. Wagner, *Appl. Phys. Lett.* **2006**, *89*, 073501.
[29] X. Wen, W. Wu, Y. Ding, Z. L. Wang, *Adv. Mater.* **2013**, *25*, 3371.
[30] C. S. Smith, *Phys. Rev.* **1954**, *94*, 42.
[31] C. Stampfer, T. Helbling, D. Obergfell, B. Schöberle, M. K. Tripp, A. Jungen, S. Roth, V. M. Bright, C. Hierold, *Nano Lett.* **2006**, *6*, 233.
[32] L. Chen, G. H. Chen, L. Lu, *Adv. Funct. Mater.* **2007**, *17*, 898.
[33] K. Lee, S. S. Lee, J. A. Lee, K.-C. Lee, S. Ji, *Appl. Phys. Lett.* **2010**, *96*, 013511.
[34] T. Yamada, Y. Hayamizu, Y. Yamamoto, Y. Yomogida, A. Izadi-Najafabadi, D. N. Futaba, K. Hata, *Nat. Nanotechnol.* **2011**, *6*, 296.
[35] Y. Wang, R. Yang, Z. Shi, L. Zhang, D. Shi, E. Wang, G. Zhang, *ACS Nano* **2011**, *5*, 3645.
[36] C. Pang, G.-Y. Lee, T.-i. Kim, S. M. Kim, H. N. Kim, S.-H. Ahn, K.-Y. Suh, *Nat. Mater.* **2012**, *11*, 795.
[37] M. Ramuz, B. C. K. Tee, J. B. H. Tok, Z. Bao, *Adv. Mater.* **2012**, *24*, 3223.

[38] C. Ye, M. Li, M. Xue, W. Shen, T. Cao, Y. Song, L. Jiang, *J. Mater. Chem.* **2011**, *21*, 5234.
[39] C. Boztug, J. R. Sanchez-Perez, F. F. Sudradjat, R. B. Jacobson, D. M. Paskiewicz, M. G. Lagally, R. Paiella, *Small* **2013**, *9*, 622.
[40] C.-A. Di, F. Zhang, D. Zhu, *Adv. Mater.* **2013**, *25*, 313.
[41] I. Lee, H. J. Sung, *Exp. in Fluids* **1999**, *26*, 27.
[42] J. Shi, M. B. Starr, X. Wang, *Adv. Mater.* **2012**, *24*, 4683.
[43] Y. Zhang, Y. Liu, Z. L. Wang, *Adv. Mater.* **2011**, *23*, 3004.
[44] O. Frank, G. Tsoukleri, I. Riaz, K. Papagelis, J. Parthenios, A. C. Ferrari, A. K. Geim, K. S. Novoselov, C. Galiotis, *Nat. Commun.* **2011**, *2*, 255.
[45] R. Holm, E. Holm, Electric Contacts: Theory and Application, Springer-Verlag, New York **1967**.
[46] L. H. Chen, S. Jin, T. H. Tiefel, *Appl. Phys. Lett.* **1993**, *62*, 2440.
[47] Q. Gao, H. Meguro, S. Okamoto, M. Kimura, *Langmuir* **2012**, *28*, 17593.
[48] T.-B. Xu, N. Guerreiro, J. Hubbard, J. H. Kang, C. Park, J. Harrison, *Appl. Phys. Lett.* **2009**, *94*, 233503.
[49] H. Zhang, X. Tao, T. Yu, S. Wang, *Sens. Actuator A-Phys.* **2006**, *126*, 129.
[50] W. Lu, M. Zu, J.-H. Byun, B.-S. Kim, T.-W. Chou, *Adv. Mater.* **2012**, *24*, 1805.
[51] N. O. Weiss, H. Zhou, L. Liao, Y. Liu, S. Jiang, Y. Huang, X. Duan, *Adv. Mater.* **2012**, *24*, 5782.
[52] D. Wu, F. Zhang, H. Liang, X. Feng, *Chem. Soc. Rev.* **2012**, *41*, 6160.
[53] Z. L. Wang, *Adv. Mater.* **2012**, *24*, 4632.
[54] K. Liu, M. Sakurai, M. Aono, *Small* **2012**, *8*, 3599.
[55] G. A. Sotiriou, C. O. Blattmann, S. E. Pratsinis, *Adv. Funct. Mater.* **2013**, *23*, 34.
[56] G. Huang, Y. Mei, *Adv. Mater.* **2012**, *24*, 2517.
[57] P. Lee, J. Lee, H. Lee, J. Yeo, S. Hong, K. H. Nam, D. Lee, S. S. Lee, S. H. Ko, *Adv. Mater.* **2012**, *24*, 3326.
[58] L. Jiang, X. Wang, L. Chi, *Small* **2011**, *7*, 1309.
[59] L. Jiang, S. Yinghui, H. Peng, L.-J. Li, T. Wu, J. Ma, F. Y. C. Boey, X. Chen, L. Chi, *Small* **2011**, *7*, 1949.
[60] Y. Xu, F. Zhang, X. Feng, *Small* **2011**, *7*, 1338.
[61] D. Chandra, S. Yang, *Acc. Chem. Res.* **2010**, *43*, 1080.
[62] C. Liu, *Adv. Mater.* **2007**, *19*, 3783.
[63] H. Münstedt, *Polymer* **1986**, *27*, 899.
[64] K. G. Neoh, T. T. Young, E. T. Kang, K. L. Tan, *J. Appl. Polym. Sci.* **1997**, *64*, 519.
[65] Q. Pei, R. Qian, *Synt. Met.* **1991**, *45*, 35.
[66] J. Fink, B. Scheerer, W. Wernet, M. Monkenbusch, G. Wegner, H. J. Freund, H. Gonska, *Phys. Rev. B* **1986**, *34*, 1101.
[67] G. Sui, J. Wang, C.-C. Lee, W. Lu, S. P. Lee, J. V. Leyton, A. M. Wu, H.-R. Tseng, *Anal. Chem.* **2006**, *78*, 5543.

Received: November 20, 2013
Published online: January 25, 2014

